

# HyperKAN: Kolmogorov-Arnold Networks make Hyperspectral Image Classifiers Smarter

Nikita Firsov<sup>1</sup>, Evgeny Myasnikov<sup>1</sup>, Valeriy Lobanov<sup>1,2</sup> Roman Khabibullin<sup>1</sup> and Artem Nikonorov<sup>1</sup>

<sup>1</sup> Samara National Research University, Samara, Russia;  
<sup>2</sup> Adyge State University, Maykop, Republic of Adygea, Russia;  
\* Correspondence: firsov.na98@gmail.com;

**Abstract:** In traditional neural network designs, a multilayer perceptron (MLP) is typically employed as a classification block following the feature extraction stage. However, the Kolmogorov-Arnold Network (KAN) presents a promising alternative to MLP, offering the potential to enhance prediction accuracy. In this paper, we study KAN-based networks for pixelwise classification of hyperspectral images. Initially, we compare baseline MLP and KAN networks with varying numbers of neurons in their hidden layers. Subsequently, we suggest replacing the linear, convolutional, and attention layers of traditional neural networks with their KAN-based counterparts. Specifically, we modify six cutting-edge neural networks, including 1D (1DCNN), 2D (2DCNN) and 3D convolutional networks (two different 3DCNNs, NM3DCNN), as well as transformer (SSFTT). Experiments conducted using seven publicly available hyperspectral datasets demonstrated a substantial improvement in classification accuracy across all the networks. The best classification quality was achieved using a KAN-based transformer architecture. Our code is available at <https://github.com/f-neumann77/HyperKAN>.

Keywords: Kolmogorov-Arnold Networks; Hyperspectral Imaging; Classification; Transformers; Convolutional Neural Networks

---

## 1. Introduction

A hyperspectral image (HSI) is a three-dimensional structure with two spatial and one spectral coordinates. Unlike RGB and multispectral images, hyperspectral images are recorded at a much higher spectral resolution. Each material, which has a unique spectral signature that serves as a “fingerprint,” can be uniquely identified in a hyperspectral image [1, 2]. This allows one to perform analysis tasks such as classification of objects on HSI, segmentation, clustering, object detection, tracking changes in time series, etc., with higher quality compared to conventional RGB or multispectral images.

The most important task of HSI analysis is the task of pixelwise classification, which involves assigning class labels to image pixels based on their spectral characteristics. This kind of task is widely in demand in remote sensing, particularly for agricultural problems [3], environmental monitoring [4], cartography [5] (for example, determining the boundaries of reservoirs [5] and glaciers [6]), etc.

Since HSIs contain both spatial and detailed spectral information about the captured scene, analysis, particularly the classification of such images, requires special tools [7]. To solve problems of HSI analysis, classical methods were used, namely the Spectral Angle Mapper (SAM) [8], spectral indices (NDVI, NDWI, etc.) [9], and others. In addition, general-purpose machine learning methods were utilized, such as SVM [10], decision trees [11], random forest [12], etc. However, such methods do not take into account spatial information contained in the HSI, and, moreover, cannot extract deeper dependencies in spectral data.

To extract deep features from spectral data more efficiently, deep architectures have been used. These architectures were based on convolutional neural networks, namely 1D networks [13], as well as based on the increasingly popular transformer architectures (see, for example, [14]).

---

To take into account spatial information, it is necessary to use deep learning tools based on spatial or spatial-spectral feature extractors. Such extractors were built based on two-dimensional convolutional layers (see, for example, 2D networks [15]) or three-dimensional convolutional layers (see 3D networks [16]). This allows a significant increase in classification quality in some cases compared to approaches that use exclusively spectral data.

Unfortunately, deep neural networks require huge amounts of data to train. HSI labeling is very labor-intensive, as it is often associated with ground-based measurements, which imposes restrictions on the use of deep neural networks for HSI analysis. For this reason, the ability of a neural network to learn from a small amount of data is an important aspect.

The deep learning algorithms are rapidly evolving, with significant advancements being made in new architectural designs. One example is networks based on the Kolmogorov-Arnold theorem [17], which have shown high efficiency in deep learning tasks. Such networks are called Kolmogorov-Arnold networks (KAN).

For example, in the paper [18] authors show that KANs outperform conventional Multi-Layer Perceptrons (MLPs) in a real-world satellite traffic forecasting task, providing more accurate results with considerably fewer learnable parameters. In the article [19], the authors show that KAN offers a promising alternative for efficient image analysis in the remote sensing field. In the paper [20], the authors show that KAN significantly outperforms MLP in terms of accuracy and convergence speed for numerous partial differential equations in computational solid mechanics, except for the complex geometry problem. In the paper [21] preliminary results indicate that while KANs are on par with MLPs in classification tasks, they seem to have a clear advantage in the graph regression tasks.

The purpose of this paper is to demonstrate the feasibility of replacing classical layers with their KAN analogs to improve the quality of HSI classification. This paper makes the following contributions:

- We study the performance of classical MLP and new KAN networks with different numbers of neurons in the hidden layer, show the advantage of KAN networks, and demonstrate the positive effect of Batch-norm in solving the problem of pixelwise HSI classification;
- We take six neural network architectures (1DCNN [22], 2DCNN [36], 3DCNN [23], 3DCNN [24], NM3DCNN [25], SSFTT [26]) for HSI classification and transform them using KAN blocks, thus obtaining six corresponding KAN-based architectures;
- Using seven different open HSI datasets we prove the advantage of each of the six KAN-based architectures over their classical counterparts, solving the problem of pixelwise HSI classification.

We describe the contributions in detail below. In Section 2, we briefly describe the replaceable blocks of classical neural networks and their KAN analogs. Next, we consider six different neural network architectures. In the same section, we show how these architectures can be transformed using KAN blocks and propose corresponding KAN-based architectures. In the third section, we briefly describe seven hyperspectral datasets used in the study, as well as the experimental conditions. Next, we show the results of a study for all the neural networks considered in Section 2 and discuss the experimental results in detail. The work ends with a conclusion and a list of references.

## 2. Materials and Methods

Typical neural network architectures for hyperspectral image classification can be described by a two-block scheme consisting of:

- Deep feature extractor;
- Classifying block (based on MLP or single linear layer).

In contrast to MLPs, which have fixed activation functions on nodes (neurons), KANs have learnable activation functions on edges (weights). KANs do not use linear weights; instead, each weight parameter is replaced by a one-dimensional function parameterized as a spline. This approach allows KAN to achieve better accuracy and interpretability compared to MLP [17]. Also utilizing KAN in traditional architectures such as U-Net [27] leads to improved quality indicators.

In this paper, we modify both the classifying block and the feature extraction block through the use of KAN-based layers. The study focuses on several architectures including simple MLP, one-dimensional, two-dimensional, and three-dimensional convolutional architectures, and a transformer. We believe that these modifications will improve the classification quality indicators.

### 2.1. KAN blocks

Let's look at how modifications were made. The classifying block was modified to include KAN layers instead of the original configuration. We will refer to this block as the Linear-KAN Block [17]. Similarly, the linear layers in an attention mechanism or convolutional layers in the feature extractor block may need to be replaced with KAN analogs.

### 2.1.1. Linear-KAN Block

The Linear-KAN Block is designed to replace the classification block in traditional neural network architectures. The architecture of the block consists of the same number of KAN-based layers as in the replaced MLP block, with each KAN-based layer preceded by a BatchNorm1D layer.

We utilized the code of the block from the Efficient KAN project [28], which sped up the original pyKAN implementation [29].

### 2.1.2. Conv-KAN Block

The Conv-KAN block is designed to replace the N-dimensional convolutional layer in the feature extractor of traditional neural network architectures. The idea is to replace linear multiplication operations with their KAN counterparts [30].

We used the implementation from the FastKAN-Conv project [31], based on Radial Basis Function.

### 2.1.3 KAN-Transformer Block

The KAN-Transformer Block is used to replace two fully connected linear layers within the Attention Block and the MLP Block of the original SSFTT architectural design.

This is achieved through the utilization of the KAN-GPT implementation [35], which enables the maintenance of the identical input and output dimensions as observed in the original SSFTT implementation for both the Attention and MLP blocks.

## 2.2. Architectures

To demonstrate the effectiveness of the KAN blocks described above, we selected the following neural network architectures utilized in literature for HSI classification:

- MLP;
- 1DCNN [22];
- 2DCNN [36];
- 3DCNN [23];
- 3DCNN [24] and its modification NM3DCNN [25];
- SSFTT [26].

In each of these architectures, we replaced the classification layers with Linear-KAN Block of the same size. Also, we replaced the layers in the Attention mechanism with the Linear-KAN blocks and convolutional layers with the Conv-KAN blocks. For all KAN layers, we experimentally choose PReLU as an activation function and a grid size of two. The remaining KAN parameters were adopted from the original implementation [28] as follows:

- Spline order = 3;
- Scale noise = 0.1;
- Scale base = 1.0;
- Scale spline = 1.0;
- Grid eps = 0.02;
- Grid range = [-1, 1]).

### 2.2.1. MLP KAN

Since MLP remains relevant and is employed in various modifications in HSI classification [32- 34], we took it as a baseline architecture. In particular, we implemented a classic multilayer perceptron containing one hidden layer. In our studies, we varied the size of the hidden layer and considered layers consisting of 16 and 128 neurons.

As an alternative to MLP, we also used a Linear-KAN block with the same number of parameters. Also, we utilized BatchNorm layers to increase the quality of classification.

### 2.2.2. 1DCNN

The 1DCNN architecture was proposed by Wei Hu and others in their paper [22] in 2015. The main concept of the paper involves using one-dimensional convolutional layers to extract deep spectral features, followed by the use of MLP to address the problem of HSI classification. The architecture comprises a one-dimensional convolutional layer, a Max Pooling layer, and two fully connected layers (refer to Figure 1a). It is worth noting that this neural network operates exclusively with spectral data and does not use spatial relationships.

The proposed modification (hereinafter referred to as 1DCNN KAN) to the 1DCNN architecture described above involves replacing the classifying block, which consists of hidden and classifying fully connected layers, with a Linear-KAN block as well as replacing the one-dimensional convolution layer in the feature extractor block with a

Conv-KAN one-dimensional layer. The Linear-KAN block has similar input and output dimensions and consists of two hidden layers of size 512. The Linear-KAN block is preceded by the Batch Norm1D layer (refer to Figure 1b).

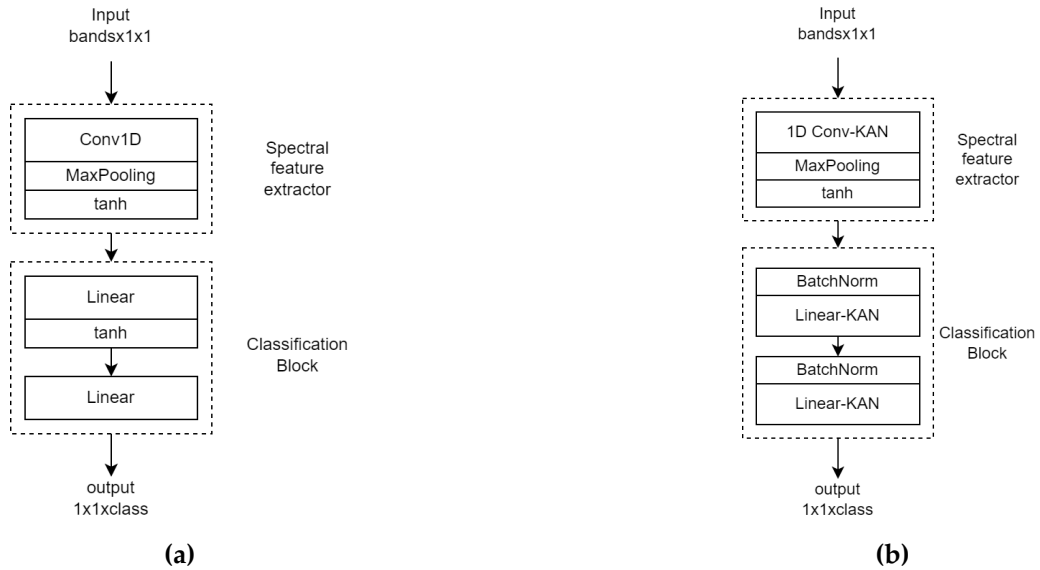


**Figure 1.** The architecture of 1DCNN (a) and the proposed modification 1DCNN KAN (b).

### 2.2.3. 2DCNN

The 2DCNN architecture was proposed by Konstantinos Makantasis and others in 2015 [36]. The main concept of the paper involves using two-dimensional convolutional layers to extract deep spatial features from hyperspectral images. The input 2D convolutional layer has a 3x3 window size and the number of convolutional kernels is 3 times the number of spectral bands. The second two-dimensional convolutional layer has a 3x3 window and the number of convolutional kernels is 3 times the number of kernels in the preceding convolutional layer. The classification block consists of two linear layers (see Figure 2a). The number of neurons in a hidden layer of a classifier is six times the number of spectral bands.

We propose to replace the two-dimensional convolutional layers with their KAN analogs, as well as the classifying block with a Linear-KAN block having 128 neurons in the hidden layer.

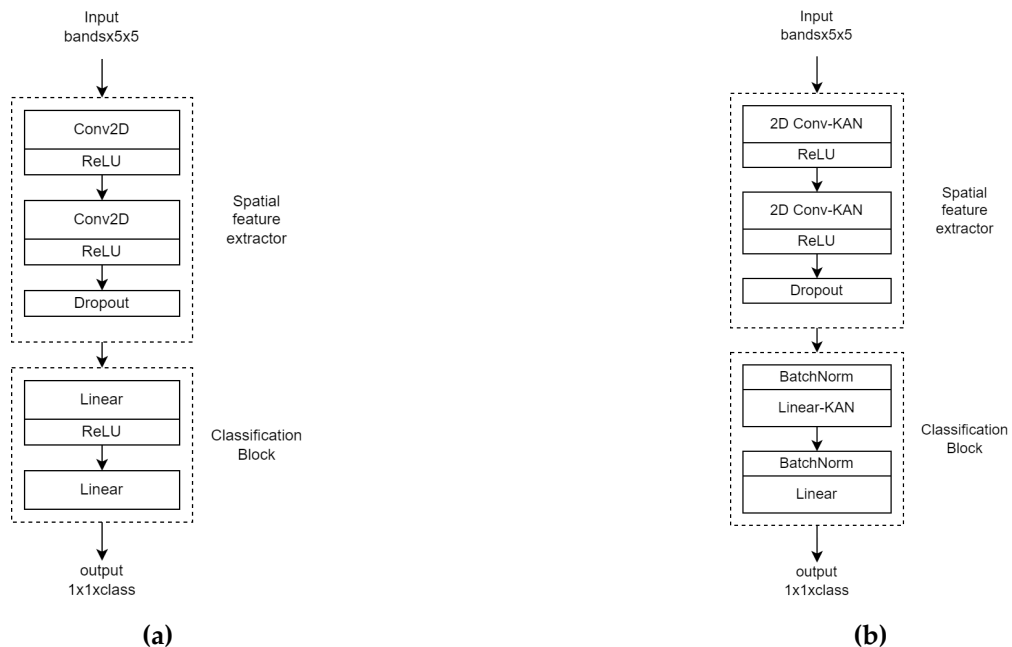


**Figure 2.** The architecture 2DCNN Luo (a) and the proposed modification 2DCNN KAN (b)

#### 2.2.4. 3DCNN by Luo

The 3DCNN architecture proposed by Yanan Luo and others in 2018 [23] combines 3D and 2D convolutional layers to extract deep spatial-spectral features. The architecture consists of an input 3D convolutional layer with a  $24 \times 3 \times 3$  window, a two-dimensional convolutional layer with a  $3 \times 3$  window, and two linear layers in a classifier (see Figure 3a).

In this paper, we propose to replace convolutional layers with their KAN analogs with fewer convolution kernels (in the original version, the number of kernels was 90 and 64 for 3D and 2D convolutional layers, respectively; in the KAN modification, the number of kernels in the corresponding layers became 64 and 32). In addition, we replaced the classification block as described above (see Figure 3b).

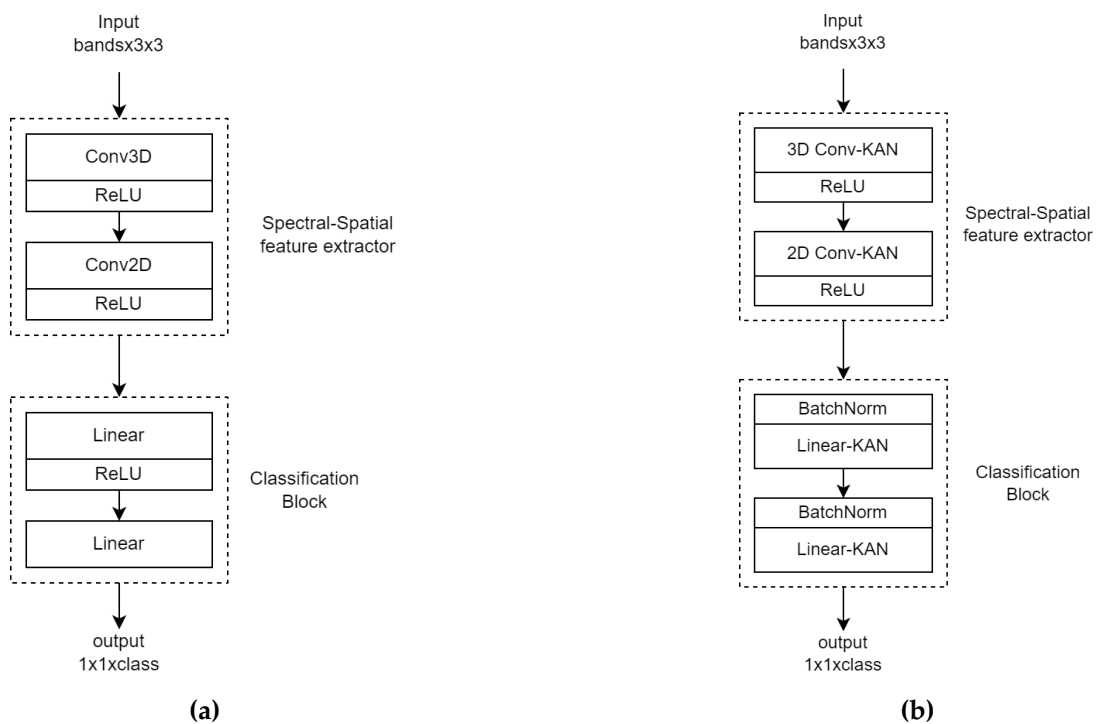


**Figure 3.** The architecture 3DCNN Luo (a) and the proposed modification 3DCNN Luo KAN (b).

#### 2.2.5. 3DCNN by He

The 3DCNN He architecture was introduced by Mingyi He and others in their paper [24] in 2017. The main idea of the paper is the use of three-dimensional convolutions to extract spectral-spatial features and the utilization of blocks of parallel one-dimensional convolutions.

The architecture comprises a three-dimensional convolutional layer for extracting primary spectral-spatial features, subsequent two blocks of four parallel convolutional layers (ConvBlock) with different convolution kernel sizes to extract more diverse spectral-spatial features of the data (refer to Figure 4a), another three-dimensional convolutional layer and a fully connected classifying layer (refer to Figure 5a).

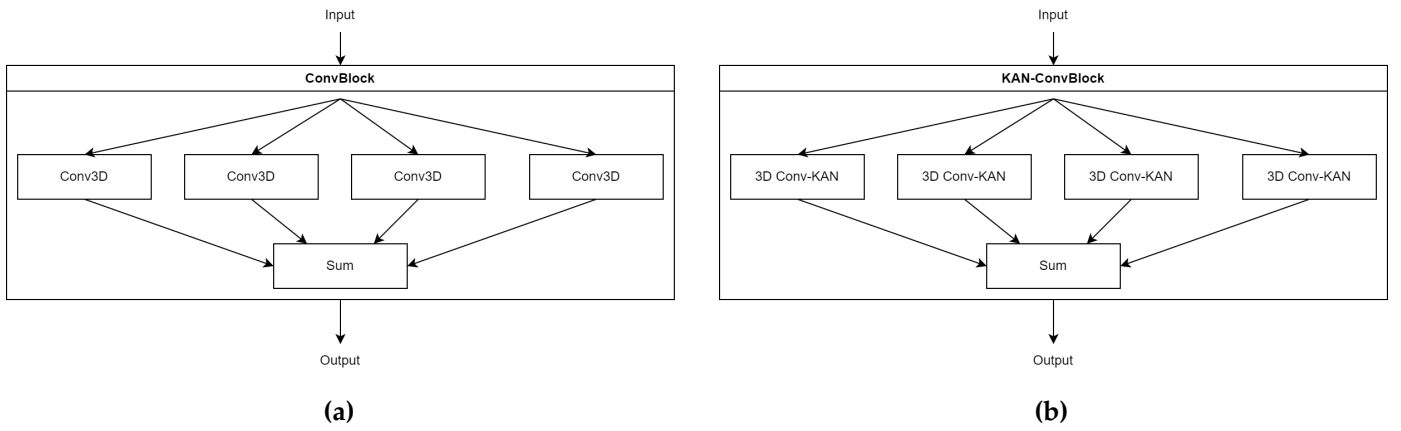


**Figure 4.** The architecture of ConvBlock (a) and the proposed modification KAN-ConvBlock (b).

The proposed modification (hereinafter referred to as 3DCNN He KAN) of the 3DCNN He architecture (as shown in Figure 5b) involves replacing all convolutional layers with Conv-KAN blocks, the ConvBlocks (see Figure 4a) with KAN-ConvBlocks (see Figure 4b), and the fully connected classification layer with Linear-KAN block possessing similar input and output dimensions. The classification block in the proposed modification contains one Linear-KAN layer with the same size as in the original version, and the BatchNorm layer preceding it.

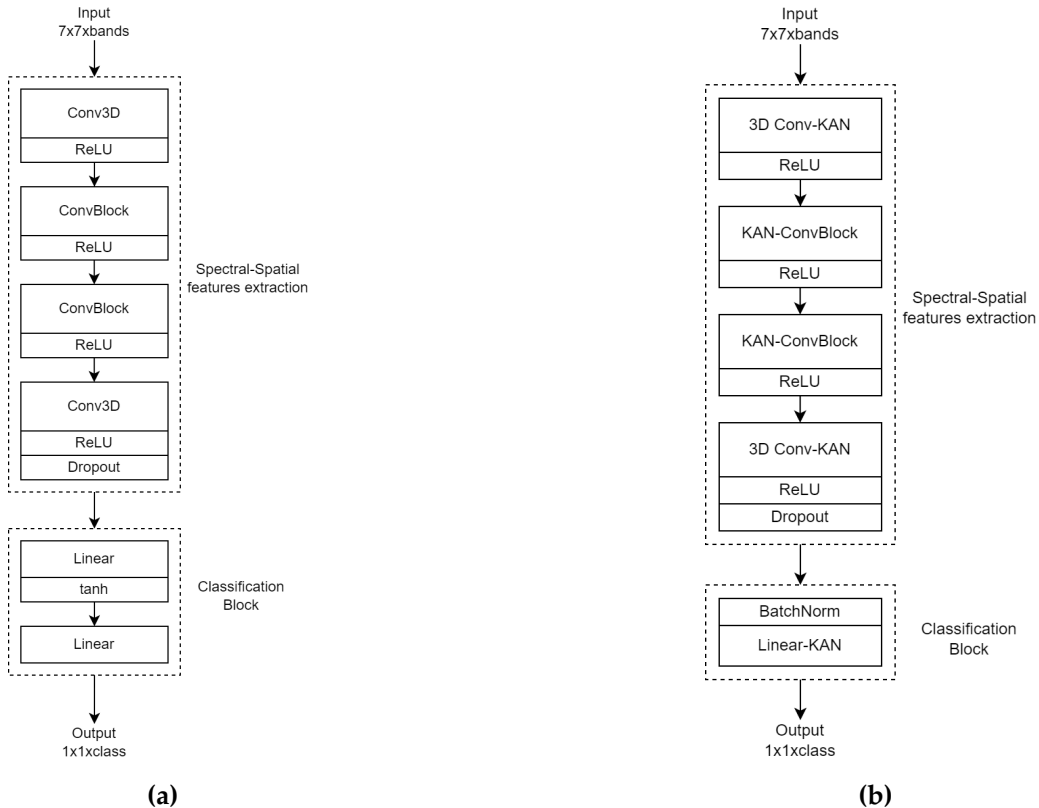


**Figure 5.** The architecture of 3DCNN He [24] (a) and the proposed modification 3DCNN He KAN (b).

## 2.2.6. NM3DCNN

The NM3DCNN architecture [25] introduced by Firsov N.A. and others in 2021 is a modification of the described earlier 3DCNN He architecture. The concept behind this modification (Figure 6a and Figure 7a) is to add a BatchNorm layer after each convolutional layer to stabilize training and eliminate the Dropout layer.

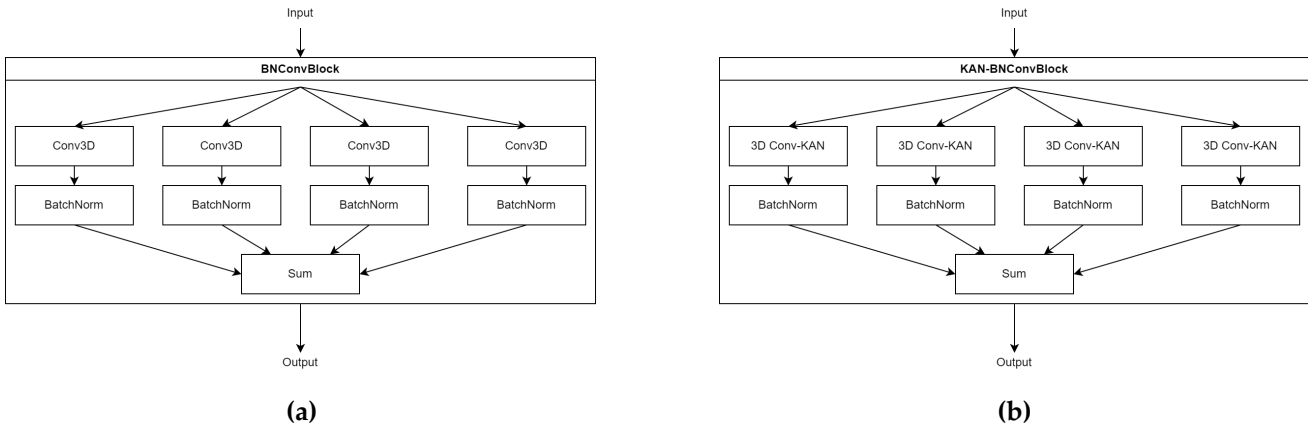


**Figure 6.** The architecture of BNConvBlock **(a)** and the proposed modification KAN-BNConvBlock **(b)**.

The modification of the NM3DCNN architecture proposed in this paper (hereinafter referred to as NM3DCNN-KAN) includes replacing all three-dimensional convolutional layers with the Conv-KAN blocks, the BNConvBlocks (see Figure 7a) with the KAN-BNConvBlocks (see Figure 7b), the fully connected classification layer with the Linear-KAN block having the same input and output dimensions and containing one layer with the same size as in the original version, and the BatchNorm1D layer preceding it (see Figure 7b). The number of kernels in all convolutional layers has been reduced by half.

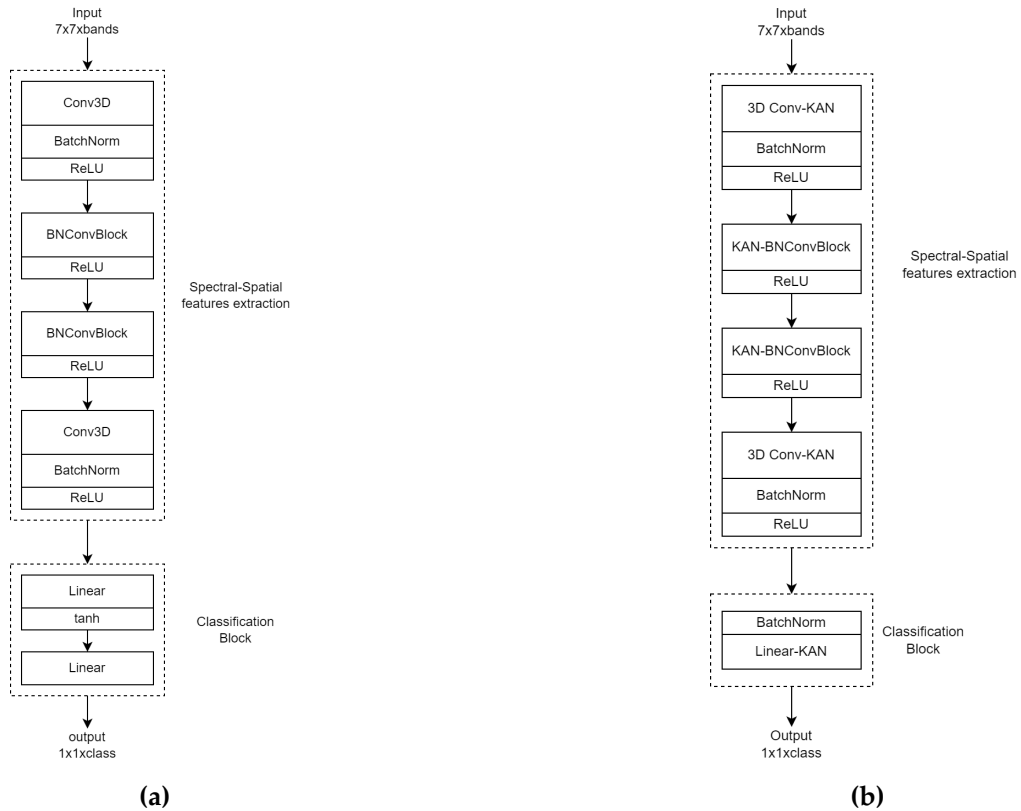


**Figure 7.** The architecture of NM3DCNN (a) and the proposed modification NM3DCNN KAN (b).

### 2.2.7. SSFTT

The SSFTT transformer architecture [26] proposed by Le Sun and others in 2022 is a combination of a spatial-spectral feature extractor, a tokenizer, a transformer encoder, and a classifying linear layer. The advantage of this architecture is the use of convolutional layers to extract spatial-spectral features along with a trainable tokenizer equipped with an attention mechanism (refer to Figure 8a).

The proposed modification (hereinafter referred to as SSFTT KAN) of the SSFTT architecture includes the following (Figure 8b):

- The replacement of the convolutional layers in the feature extractor with Conv-KAN blocks, maintaining the input and output dimensions.
- The replacement of two fully connected layers within the Attention block with a Linear-KAN block consisting of two layers of the same size as the original version, while preserving the input and output dimensions (taken from the KAN GPT implementation [35]);
- The replacement of two fully connected linear layers within the Encoder with a Linear-KAN block containing two layers of the same size as the original version, maintaining the input and output dimensions of the MLP block (taken from the KAN GPT implementation [35], as this implementation is intended for transformer architectures);
- The replacement of the classification block with the Linear-KAN block, containing the only linear-KAN layer of the same size as the original version.

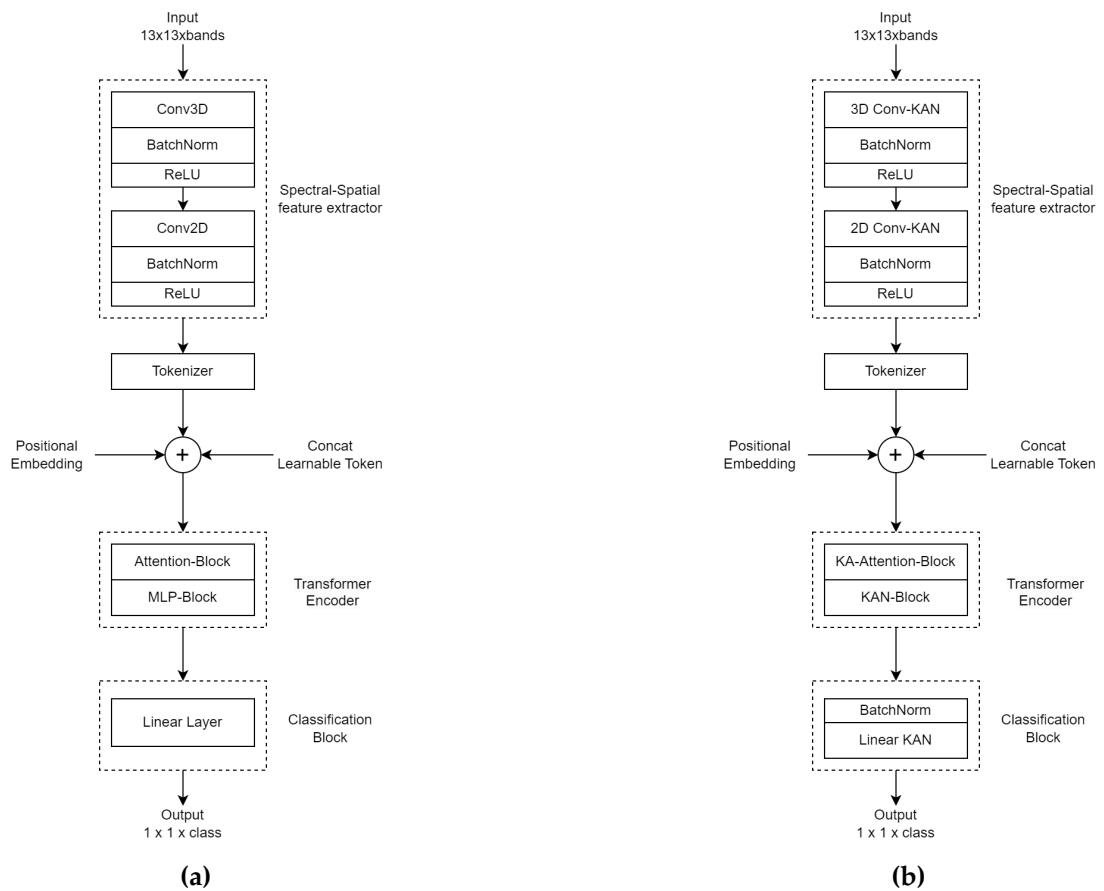


**Figure 8.** The SSFTT architecture (a) and the proposed modification of the SSFTT architecture (b).

### 3. Results

#### 3.1. Description of datasets

In our study, we used seven different open hyperspectral datasets listed in Table 1 along with their characteristics.

For the Pavia University and Indian Pines scenes, we chose 20% of random pixels from each class for the training set. For the remaining datasets (PaviaC, Salinas, Houston 13, Houston 18, and KSC) we chose 10% of random pixels from each class. Consequently, the test set consisted of 80% of the data for PaviaU and Indian Pines and 90% for the other datasets. The strategy for choosing such a data partition was based on the search for the optimal architecture of a neural network classifier that could work on a small set of training data.

For the SSFTT architecture, the PCA technique was applied with the reduction to 30 components, as it was done in the original paper.

**Table 1.** Datasets.

Dataset Name	Size	Spectral channels	Number of classes	Classes
PaviaU	610x340	103	9	Void, Asphalt, Meadows, Gravel, Trees, Painted metal sheets, Bare soil, Bitumen, Self-blocking bricks, Shadows
PaviaC	1096x715	102	9	Void, Water, Trees, Meadows, Self-blocking bricks, Bare soil, Asphalt, Bitumen, Tiles, Shadows
Salinas	512x217	204	16	Void, Green weeds 1, Green weeds 2, Fallow, Fallow rough plow, Fallow smooth, Stubble, Celery, Grapes Untrained, Soil vinyard, Corn senesced, Luttuce romaine 4 wk, Luttuce romaine 5 wk, Luttuce romaine 6 wk, Luttuce romaine 7 wk, Vinyard_untrained, Vinyard_vertical
Indian Pines	145x145	200	16	Void, Alfalfa, Corn-notill, Corn-min, Corn, Grass/Pasture, Grass/Trees, Grass pasture/mowed, Hay-windrowed, Oats, Soybeans-no till, Soybeans-min till, Soybeans-clean till, Wheat, Woods, Buildings-grass-trees-Drive, Store-steel-towers
Houston 13	954x210	48	7	Void, Grass healthy, Grass stressed, Trees, Water, Residential Buildings, Non-residential Buildings, Road
Houston 18	954x210	48	7	Void, Grass healthy, Grass stressed, Trees, Water, Residential Buildings, Non-residential Buildings, Road
KSC	512x614	176	13	Void, Scrub, Willow swamp, CP hammock, Slash pine, Oak/Broadleaf, Hardwood, Swamp, Graminoid marsh, Spartina marsh, Cattail marsh, Salt marsh, Mud flats, Water

### 3.2. Experimental results

In the first stage of experiments, we investigated MLP and KAN as baseline approaches, which exclusively process spectral features (pixels of hyperspectral images) and do not incorporate any spatial context. Both MLP and KAN were taken with one hidden layer, varying the size between 16 and 128. We also considered adding batch normalization (BN) before each layer. The results of these experiments are shown in Table 2. In the last two columns, for each pair of MLP and KAN neural networks, we present the classification quality averaged across all used datasets, as well as the classification quality gain obtained with KAN.

As can be seen, KAN architectures showed better results than similar MLPs. The greatest difference in the classification accuracy is achieved for fewer neurons without using normalization. At the same time, normalization itself has a noticeable positive effect on the quality of classification. When using it, the average accuracy is higher. Moreover, the average accuracy for a network with fewer parameters with normalization (for example, 16 BN) is higher than the accuracy of a network with a larger number of parameters without normalization (for example, 32), which can be caused by overfitting. The best quality values were achieved by the KAN 128 BN network for almost all the datasets.

**Table 2.** Overall classification accuracy (OA) for baseline neural network models and datasets, in percent.

Model Name	Dataset Name							Average	Average gain
	PaviaU*	PaviaC	Salinas	Indian Pines*	Houston13	Houston 18	KSC		
MLP and KAN models									
MLP 16	92.68	97.12	91.41	75.40	95.66	86.12	82.01	88.62	2.45
KAN 16	95.02	98.22	91.65	80.31	95.92	90.09	86.32	91.07	
MLP 32	94.54	98.21	91.58	78.12	96.75	87.81	84.87	90.26	1.09
KAN 32	94.88	98.69	91.84	82.02	96.10	89.47	86.45	91.35	
MLP 64	95.43	98.27	91.78	82.62	97.27	90.36	85.79	91.64	0.46

KAN 64	94.92	98.62	92.26	83.13	96.66	90.67	88.47	92.10	
MLP 128	91.66	97.72	90.07	73.63	80.72	87.00	73.13	84.84	4.55
KAN 128	94.84	98.05	91.21	83.79	96.36	90.98	88.00	89.39	
MLP and KAN models with batch normalization									
MLP 16 BN	92.85	97.91	91.16	80.28	97.09	87.25	88.38	90.70	1.25
KAN 16 BN	95.81	98.66	93.56	80.63	94.84	89.50	90.70	91.95	
MLP 32 BN	94.49	98.29	92.66	84.08	97.27	89.46	90.02	92.32	0.5
KAN 32 BN	95.12	98.61	94.26	83.32	96.96	90.34	91.14	92.82	
MLP 64 BN	95.69	98.47	92.98	85.77	97.01	89.92	91.03	92.98	0.6
KAN 64 BN	96.14	98.98	93.70	<b>87.86</b>	96.53	91.24	90.61	93.58	
MLP 128 BN	95.92	98.65	93.53	86.35	97.53	90.07	<b>91.73</b>	93.39	0.52
KAN 128 BN	<b>96.34</b>	<b>99.03</b>	<b>94.22</b>	87.01	<b>97.57</b>	<b>92.04</b>	91.22	<b>93.91</b>	

\* The training sample size for PaviaU and Indian Pines consisted of 20% samples per class, while for other datasets it was 10% per class.

In the second stage of experiments, we investigated the efficiency of the complete replacement of classical layers with their KAN analogs in convolutional and transformer networks. We performed the replacement both in the feature extractor blocks (convolutional layers) and in the transformer attention and MLP blocks. The classifying block of linear layers was also replaced with a similar KAN block.

We standardized the data at the preprocessing stage. For both SSFTT and SSFTT KAN networks, the principal component analysis (PCA) technique was used to extract the first 30 principal components.

All the models were trained until the training accuracy and loss indicators reached a plateau. The learning rate was selected from the range [0.001, 0.4]. We used the Adam optimizer and selected the scheduler parameters based on convergence. The hyperparameter selection for training KAN networks is similar to classical architectures, except for faster convergence.

All the described models were trained from scratch.

The results of the experiments are presented in Tables 3 and 4.

We grouped the results for the specified architectures based on the convolution type and window size used by the networks to extract features. The architectures 1DCNN and 1DCNN KAN use spectral features only and do not use any spatial context, while 2DCNN and 2DCNN KAN utilize 2D convolutions of spatial data. 3DCNN Luo and 3DCNN Luo KAN utilize spectral-spatial convolutions with 3x3 spatial window. 3DCNN He, 3DCNN He KAN, NM3DCNN and NM3DCNN KAN utilize a 7x7 spatial window. SSFTT and SSFTT KAN, stand apart, with the spatial patch sizes for these networks being 13x13.

As earlier, in the last two columns, we present the classification quality and gain averaged over all used datasets for each pair of original and KAN-based networks.

**Table 3.** Overall classification accuracy (OA) for various neural network models and datasets, in percent.

Model Name	Dataset Name							Average	Average gain
	PaviaU*	PaviaC	Salinas	Indian Pines*	Houston13	Houston 18	KSC		
Convolutions of spectral features									
1DCNN	95.17	98.20	91.93	85.82	92.63	91.32	84.87	91.42	
1DCNN KAN	<b>95.68</b>	<b>99.07</b>	<b>95.28</b>	<b>88.90</b>	<b>96.88</b>	<b>93.63</b>	<b>90.91</b>	<b>94.33</b>	2.92
Convolutions of spatial features (window size 3x3)									
2DCNN	97.93	99.03	93.10	86.56	93.78	93.19	84.72	92.61	
2DCNN KAN	<b>99.12</b>	<b>99.57</b>	<b>96.52</b>	<b>93.77</b>	<b>95.97</b>	<b>94.26</b>	<b>86.19</b>	<b>95.05</b>	2.44
Convolutions of spectral-spatial features (window size 3x3)									
3DCNN Luo	96.92	99.21	93.99	81.90	95.69	92.45	87.37	92.50	
3DCNN Luo KAN	<b>99.02</b>	<b>99.57</b>	<b>96.97</b>	<b>91.33</b>	<b>96.77</b>	<b>94.16</b>	<b>90.72</b>	<b>95.50</b>	3.00
Convolutions of spectral-spatial features (window size 7x7)									
3DCNN He	98.05	97.39	93.03	84.45	90.40	91.98	88.87	92.02	
3DCNN He KAN	<b>98.76</b>	<b>99.71</b>	<b>98.14</b>	<b>96.47</b>	<b>97.04</b>	<b>95.82</b>	<b>93.66</b>	<b>97.08</b>	5.05
NM3DCNN	99.33	99.57	96.78	90.20	94.41	95.53	86.61	94.63	
NM3DCNN KAN	<b>99.52</b>	<b>99.75</b>	<b>98.01</b>	<b>95.39</b>	<b>97.53</b>	<b>95.84</b>	<b>94.40</b>	<b>97.20</b>	2.57
Convolutions of spectral-spatial features (window size 13x13), 30 principal components									
SSFTT	99.86	99.88	99.85	98.78	98.57	96.22	95.45	98.37	
SSFTT KAN	<b>99.92</b>	<b>99.93</b>	<b>99.97</b>	<b>99.24</b>	<b>99.46</b>	<b>97.12</b>	<b>98.76</b>	<b>99.20</b>	0.8271

\* The training sample size for PaviaU and Indian Pines consisted of 20% samples per class, while for other datasets it was 10% per class.

**Table 4.** Weighted F1 measure for various neural network models and datasets.

Model Name	Dataset Name							Average	Average gain
	PaviaU*	PaviaC	Salinas	Indian Pines*	Houston13	Houston 18	KSC		
Convolutions of spectral features									
1DCNN	0.9524	0.9811	0.9165	0.8577	0.9262	0.9125	0.8469	0.9133	
1DCNN KAN	<b>0.9566</b>	<b>0.9903</b>	<b>0.9525</b>	<b>0.8883</b>	<b>0.9680</b>	<b>0.9356</b>	<b>0.9088</b>	<b>0.9428</b>	0.0295
Convolutions of spatial features (window size 3x3)									
2DCNN	0.9788	0.9898	0.9307	0.8640	0.9366	0.9311	0.8465	0.9253	
2DCNN KAN	<b>0.9910</b>	<b>0.9951</b>	<b>0.9646</b>	<b>0.9353</b>	<b>0.9581</b>	<b>0.9423</b>	<b>0.8606</b>	<b>0.9495</b>	0.2442
Convolutions of spectral-spatial features (window size 3x3)									
3DCNN Luo	0.9689	0.9914	0.9392	0.8185	0.9563	0.9243	0.8728	0.9244	
3DCNN Luo KAN	<b>0.9898</b>	<b>0.9949</b>	<b>0.9690</b>	<b>0.9130</b>	<b>0.9672</b>	<b>0.9413</b>	<b>0.9067</b>	<b>0.9545</b>	0.0300
Convolutions of spectral-spatial features (window size 7x7)									
3DCNN He	0.9801	0.9737	0.9301	0.8442	0.9036	0.9195	0.8882	0.9199	
3DCNN He KAN	<b>0.9874</b>	<b>0.9968</b>	<b>0.9813</b>	<b>0.9646</b>	<b>0.9700</b>	<b>0.9577</b>	<b>0.9364</b>	<b>0.9706</b>	0.0506
NM3DCNN	0.9929	0.9954	0.9676	0.9014	0.9437	0.9552	0.8660	0.9460	
NM3DCNN KAN	<b>0.9951</b>	<b>0.9973</b>	<b>0.9800</b>	<b>0.9537</b>	<b>0.9751</b>	<b>0.9583</b>	<b>0.9438</b>	<b>0.9719</b>	0.0258
Convolutions of spectral-spatial features (window size 13x13), 30 principal components									
SSFTT	0.9985	0.9987	0.9985	0.9877	0.9856	0.9621	0.9543	0.9836	
SSFTT KAN	<b>0.9990</b>	<b>0.9992</b>	<b>0.9996</b>	<b>0.9923</b>	<b>0.9945</b>	<b>0.9712</b>	<b>0.9875</b>	<b>0.9919</b>	0.008271

\* The training sample size for PaviaU and Indian Pines consisted of 20% samples per class, while for other datasets it was 10% per class.

#### 4. Discussion

All considered solutions provided a fairly high level of quality. Let's start the analysis with classical architectures.

Among convolutional networks with a traditional architecture the 1DCNN network that use only spectral information showed the weakest results on average. The 2DCNN network based on convolution of spatial features was on average 1% better compared to 1DCNN. It showed similar or slightly better results on all the considered scenes. This demonstrates the importance of using local spatial context when analyzing hyperspectral remote sensing images.

Among the networks based on spectral-spatial convolutions (3DCNN Luo, 3DCNN He, NM3DCNN), we prefer the NM3DCNN. It showed the best results for almost all the analyzed scenes (except Houston13 and KSC) and provided a significant increase in quality for the Indian Pines scene (5.75% against 3DCNN He and 8.3% against 3DCNN Luo. This network also showed better results than the networks based on convolutions of spectral or spatial features (1DCNN and 2DCNN).

The results obtained by SSFTT are noticeably higher than for other classical neural networks considered. The greatest difference is achieved for the Indian Pines and KSC scenes (8.58% and 8.84% against NM3DCNN, correspondingly). We suspect that the significantly larger spatial window (context) size is the main reason for this difference.

The primary objective of this study was not to compare different neural network architectures, but instead to highlight the advantages of KAN-based architectures over their traditional counterparts. Let's take a look at the results obtained by the neural networks based on KAN blocks.

The results show that replacing traditional layers with KAN analogs is appropriate. An improvement in quality compared to traditional architectures was observed in all the considered cases. For convolutional neural networks, the average improvement across datasets was 2.44-5.05% depending on the architecture, with the largest effect achieved

for the 3DCNN He network. Although the smallest increase in quality was observed for the transformer SSFTT KAN network (the average increase was less than 1%), this network achieved the best classification quality.

The main trends described above for the classical architectures are also preserved for the corresponding KAN networks. In particular, 2DCNN KAN is on average 0.72% better than 1DCNN KAN; NM3DCNN KAN is 2.15% better than 2DCNN KAN; and SSFTT KAN is 1.99% better than NM3DCNN KAN. The highest classification accuracy (99.2%) among all the networks considered belongs to the SSFTT KAN transformer network. It is worth noting that the results obtained for the f-measure (see Table 4) generally confirm the conclusions based on the classification accuracy indicator.

In our experiments, in most cases using Linear-KAN layers before MLP as the final classifying layer shows a significant increase in performance. Implementing a KAN-based convolutional layer leads to a smaller improvement in classification quality, particularly when using the Radial Basis Function and B-spline. In the case of the transformer architecture, replacing the classifying block did not significantly improve the classification accuracy. However, the replacement in the attention and MLP blocks allowed the modified transformer to increase the quality indicators. It is worth noting that using KAN layers resulted in better convergence, but training such networks takes a bit longer. We also managed to achieve the same accuracy as in traditional architectures when using KAN layers with a smaller number of neurons.

## 5. Conclusions

In this paper, we applied KAN networks for pixelwise classification of hyperspectral images. We started by replacing the traditional MLP with a recently proposed KAN network and showed the advantages of the latter. We found that incorporating batch normalization layers produced the best results.

Then, we proposed KAN equivalents for six different neural networks for HSI classification, including 1D (1DCNN), 2D (2DCNN), and 3D convolutional networks (3DCNN Luo, 3DCNN He, NM3DCNN), as well as a transformer (SSFTT). We completely replaced the classical convolutional and classification layers, as well as attention mechanisms, with the corresponding KAN analogs.

Using seven different open hyperspectral datasets, we demonstrated the superiority of the modified KAN architectures over traditional networks in all considered cases. For the convolutional networks (3DCNN Luo KAN, 3DCNN He KAN, and NM3DCNN KAN), there was an average increase in classification accuracy of 2.44–5.05%. The smallest increase in classification quality (0.83%) was observed for the transformer SSFTT KAN network, while this network showed the highest classification accuracy at 99.2% averaged across all datasets.

**Acknowledgments:** This work was supported by the Analytical Center for the Government of the Russian Federation (agreement identifier 000000D730324P540002, grant No 70-2023-001317 dated 28.12.2023).

## References

1. Lu, G.; Fei, B. Medical hyperspectral imaging: a review. *Journal of Biomedical Optics* **2014**, *19*(1), 010901. <https://doi.org/10.1117/1.JBO.19.1.010901>
2. Klein, M.E.; Aalderink, B.J.; Padoan, R.; de Bruin, G.; Steemers, T.A.G. Quantitative Hyperspectral Reflectance Imaging. *Sensors* **2008**, *8*, 5576–5618. <https://doi.org/10.3390/s8095576>
3. Wang, C.; Liu, B.; Liu, L. et al. A review of deep learning used in the hyperspectral image analysis for agriculture. *Artif Intell Rev* **2021**, *54*, 5205–5253. <https://doi.org/10.1007/s10462-021-10018-y>
4. Sun, G.; Jiao, Z.; Zhang, A.; Li, F.; Fu, H.; Li, Z. Hyperspectral image-based vegetation index (HSVI): A new vegetation index for urban ecological research. *International Journal of Applied Earth Observation and Geoinformation* **2021**, *103*, 102529. <https://doi.org/10.1016/j.jag.2021.102529>
5. Liu, C.; Tao, R.; Li, W.; Zhang, M.; Sun, W.; Du, Q. Joint Classification of Hyperspectral and Multispectral Images for Mapping Coastal Wetlands. *IEEE Journal of Selected Topics in Applied Earth Observations and Remote Sensing* **2020**, *99*, 1–15. <https://doi.org/10.1109/ISTARS.2020.3040305>
6. Sood, V.; Tiwari, R.K.; Singh, S.; Kaur, R.; Parida, B.R. Glacier Boundary Mapping Using Deep Learning Classification over Bara Shigri Glacier in Western Himalayas. *Sustainability* **2022**, *14*, 13485. <https://doi.org/10.3390/su142013485>
7. Nalepa, J. Recent Advances in Multi- and Hyperspectral Image Analysis. *Sensors* **2021**, *21*, 6002. <https://doi.org/10.3390/s21186002>
8. Chakravarty, S.; Paikaray, B.K.; Mishra R.; Dash, S. Hyperspectral Image Classification using Spectral Angle Mapper. *Proceedings of the IEEE International Women in Engineering (WIE) Conference on Electrical and Computer Engineering (WIECON-ECE)* **2021**, 87–90. <https://doi.org/10.1109/WIECON-ECE54711.2021.9829585>

9. Ju, Y.; Bohrer, G. Classification of Wetland Vegetation Based on NDVI Time Series from the HLS Dataset. *Remote Sens.* **2022**, *14*, 2107. <https://doi.org/10.3390/rs14092107>
10. Wang, Y.; Yu, W.; Fang, Z. Multiple Kernel-Based SVM Classification of Hyperspectral Images by Combining Spectral, Spatial, and Semantic Information. *Remote Sens.* **2020**, *12*, 120. <https://doi.org/10.3390/rs12010120>
11. Xu, S.; Liu, S.; Wang, H.; Chen, W.; Zhang, F.; Xiao, Z. A Hyperspectral Image Classification Approach Based on Feature Fusion and Multi-Layered Gradient Boosting Decision Trees. *Entropy* **2021**, *23*, 20. <https://doi.org/10.3390/e23010020>
12. Wang, Z.; Zhao, Z.; Yin, C. Fine Crop Classification Based on UAV Hyperspectral Images and Random Forest. *ISPRS Int. J. Geo-Inf.* **2022**, *11*, 252. <https://doi.org/10.3390/ijgi11040252>
13. Huang, J.; He, H.; Lv, R.; Zhang, G.; Zhou, Z.; Wang, X. Non-destructive detection and classification of textile fibres based on hyperspectral imaging and 1D-CNN. *Analytica Chimica Acta* **2022**, *1224*, 340238. <https://doi.org/10.1016/j.aca.2022.340238>
14. Hong, D.; Han, Z.; Yao, J.; Gao, L.; Plaza, A.; Chanussot, J. SpectralFormer: Rethinking Hyperspectral Image Classification With Transformers. *IEEE Transactions on Geoscience and Remote Sensing* **2021**, *60*, 5518615. <https://doi.org/10.1109/TGRS.2021.3130716>
15. Hsieh, T.-H.; Kiang, J.-F. Comparison of CNN Algorithms on Hyperspectral Image Classification in Agricultural Lands. *Sensors* **2020**, *20*, 1734. <https://doi.org/10.3390/s20061734>
16. Kanthi, M.; Sarma, T.; Chigarpalle, S. Multi-scale 3D-convolutional neural network for hyperspectral image classification. *Indonesian Journal of Electrical Engineering and Computer Science* **2022**, *25*, 307. <https://doi.org/10.11591/ijeecs.v25.i1.pp307-316>
17. Liu, Z.; Wang, Y.; Vaidya, S.; Ruehle, F.; Halverson, J.; Soljacic, M.; Hou, T.Y.; Tegmark, M. KAN: Kolmogorov-Arnold Networks. *arXiv preprint arXiv:2404.19756*, **2024**, 1-50. <https://doi.org/10.48550/arXiv.2404.19756>
18. Vaca-Rubio, C.J.; Blanco, L.; Pereira, R.; Caus, M. Kolmogorov-Arnold Networks (KANs) for Time Series Analysis. *arXiv preprint arXiv:2405.08790*, **2024**, 1-7. <https://doi.org/10.48550/arXiv.2405.08790>
19. Cheon, M. Kolmogorov-Arnold Network for Satellite Image Classification in Remote Sensing. *arXiv preprint arXiv: 2406.00600*, **2024**, 1-10. <https://doi.org/10.48550/arXiv.2406.00600>
20. Wang, Y.; Sun, J.; Bai, J.; Anitescu, C.; Eshaghi, M.S.; Zhuang, X.; Rabczuk, T.; Liu, Y. Kolmogorov Arnold Informed neural network: A physics-informed deep learning framework for solving PDEs based on Kolmogorov Arnold Networks. *arXiv preprint arXiv: 2406.11045*, **2024**, 1-10. <https://doi.org/10.48550/arXiv.2406.11045>
21. Bresson, R.; Nikolentzos, G.; Panagopoulos, G.; Chatzianastasis, M.; Pang, J.; Vazirgiannis, M. KAGNNs: Kolmogorov-Arnold Networks meet Graph Learning. *arXiv preprint arXiv: 2406.18380*, **2024**, 1-15. <https://doi.org/10.48550/arXiv.2406.18380>
22. Hu, W.; Huang, Y.; Wei, L.; Zhang, F.; Li, H. Deep convolutional neural networks for hyperspectral image classification. *Journal of Sensors* **2015**, *2015*, 258619. <https://doi.org/10.1155/2015/258619>
23. Luo, Y.; Zou, J.; Yao, C.; Zhao, X.; Li, T.; Bai, G. HSI-CNN: A Novel Convolution Neural Network for Hyperspectral Image. *Proceedings of International Conference on Audio, Language and Image Processing (ICALIP)* **2018**, *2018*, 464-469. <https://doi.org/10.1109/ICALIP.2018.8455251>
24. He, M.; Li, B.; Chen, H. Multi-scale 3D deep convolutional neural network for hyperspectral image classification. *Proceedings of IEEE International Conference on Image Processing (ICIP)* **2017**, *2017*, 3904-3908. <https://doi.org/10.1109/ICIP.2017.8297014>
25. Firsov, N.A.; Podlipnov, V.V.; Ivliev, N.A.; Ryskova, D.D.; Pirogov, A.V.; Muzyka, A.A.; Makarov, A.R.; Lobanov, V.; Platonov, V.I.; Babichev, A.N.; Monastyrskiy, V.A.; Olgarenko, V.I.; Nikolaev, D.P.; Skidanov, R.V.; Nikonorov, A.V.; Kazanskiy, N.L.; Soyfer, V.A. Ensembles of spectral-spatial convolutional neural network models for classifying soil types in hyperspectral images. *Computer Optics* **2023**, *47*, 795-805. <https://doi.org/10.18287/2412-6179-CO-1260>
26. Sun, L.; Zhao, G.; Zheng, Y.; Wu, Z. Spectral-spatial feature tokenization transformer for hyperspectral image classification. *IEEE Transactions on Geoscience and Remote Sensing* **2022**, *60*, 5522214. <https://doi.org/10.1109/TGRS.2022.3144158>
27. Li, C.; Liu, X.; Li, W.; Wang, C.; Liu, H.; Yuan, Y. U-KAN Makes Strong Backbone for Medical Image Segmentation and Generation. *arXiv preprint arXiv: 2406.02918*, **2024**, 1-16. <https://doi.org/10.48550/arXiv.2406.02918>
28. Efficient KAN. Available online: <https://github.com/Blealtan/efficient-kan> (accessed on 06 July 2024).
29. PyKAN. Available online: <https://github.com/KindXiaoming/pykan> (accessed on 06 July 2024).
30. ConvKAN. Available online: <https://github.com/StarostinV/convkan> (accessed on 06 July 2024).
31. <https://arxiv.org/abs/2407.01092> (accessed on 06 July 2024).
32. Lin, M.; Jing, W.; Di, D.; Chen, G.; Song, H. Multi-Scale U-Shape MLP for Hyperspectral Image Classification. *IEEE Geoscience and Remote Sensing Letters* **2022**, *19*, 6006105. <https://doi.org/10.1109/LGRS.2022.3141547>
33. Jamali, A.; Mahdianpari, M.; Abdul Rahman, A. Hyperspectral image classification using multi-layer perceptron mixer (MLP-MIXER). *Int. Arch. Photogramm. Remote Sens. Spatial Inf. Sci.* **2023**, *XLVIII-4/W6-2022*, 179–182. <https://doi.org/10.5194/isprs-archives-XLVIII-4-W6-2022-179-2023>
34. Meng, Z.; Zhao, F.; Liang, M. SS-MLP: A Novel Spectral-Spatial MLP Architecture for Hyperspectral Image Classification. *Remote Sens.* **2021**, *13*, 4060. <https://doi.org/10.3390/rs13204060>
35. KAN GPT. Available online: <https://github.com/AdityaNG/kan-gpt> (accessed on 06 July 2024).

---

36. Makantasis, K.; Karantzalos, K.; Doulamis, A.; Doulamis, N. Deep supervised learning for hyperspectral data classification through convolutional neural networks. *2015 IEEE International Geoscience and Remote Sensing Symposium (IGARSS)*, **2015**, 4959-4962. <https://doi.org/10.1109/IGARSS.2015.7326945>.